Molecular Therapy
Methods & Clinical Development
Original Article

αFAP-specific nanobodies mediate a highly precise retargeting of modified AAV2 capsids thereby enabling specific transduction of tumor tissues

Olaniyi Olarewaju,[1] Franziska Held,[1] Pamela Curtis,[2] Cynthia Hess Kenny,[2] Udo Maier,[1] Tadas Panavas,[2] and Francois du Plessis[1]

[1]AAV Gene Therapy Research Group, Research Beyond Borders (RBB), Boehringer Ingelheim Pharma GmbH & Co. KG, 88400 Biberach an der Riß, Germany; [2]Biotherapeutics Discovery, Boehringer Ingelheim Pharmaceuticals, Inc., Ridgefield, CT 06877, USA

Due to the refractiveness of tumor tissues to adeno-associated virus (AAV) transduction, AAV vectors are poorly explored for cancer therapy delivery. Here, we aimed to engineer AAVs to target tumors by enabling the specific engagement of fibroblast activation protein (FAP). FAP is a cell surface receptor distinctly upregulated in the reactive tumor stroma, but rarely expressed in healthy tissues. Thus, targeting FAP presents an opportunity to selectively transduce tumor tissues. To achieve this, we modified the capsid surface of AAV2 with an αFAP nanobody to retarget the capsid to engage FAP receptor. Following transduction, we observed a 23- to 80-fold increase in the selective transduction of FAP^+ tumor cells *in vitro*, and greater than 5-fold transduction of FAP^+ tumor tissues *in vivo*. Subsequent optimization of the VP1-nanobody expression cassette further enhanced the transduction efficiency of the modified capsids. Due to the limited αFAP nanobodies repertoires, we broadened the versatility of this high-fidelity platform by screening a naive VHH yeast display library, leading to the identification of several novel αFAP nanobody candidates (K_D = 0.1 to >100 nM). Hence, our study offers new opportunity for the application of AAV vectors for highly selective delivery of therapeutics to the tumor stroma.

INTRODUCTION

Adeno-associated virus (AAV) is member of the dependoparvovirus, characterized by a linear, single-stranded DNA genome, which is approximately 4.7 kb and flanked by inverted terminal repeats (ITRs).[1] First described as a contaminant during adenovirus production in 1965 by Robert Atchison and colleagues,[2] the prospect of AAV as a gene therapy platform soared in the early 1980s, following the successful cloning of the AAV genome into plasmid DNA.[3–5] Since then, recombinant AAV (rAAV) has emerged as the preferred *in vivo* gene therapy vehicle, scoring seven clinical approvals across broad disease indications since 2017.[6–8]

Despite the success of rAAVs in the clinic, the relatively broad tropism of rAAVs and low transduction efficiency in certain tissue types present distinct challenges.[9] To mitigate the challenge of the tissue promiscuity of AAVs, expression of the encoded transgene can be restricted to the target tissue by local injection, or the use of tissue-specific promoters to drive the transgene expression specifically in the target tissues.[10–12] Nevertheless, this does not eliminate the potential risks of accumulation of AAV particles in off-target tissues.[10,13] To address this, high-throughput directed evolution and/or rational design capsid engineering approaches have been developed to generate next-generation AAV vectors with improved target-tissue specificity. Specifically advancing to the targeted transduction of cell or tissue types that were previously refractory to AAV transduction.[12,14–17] Nanobodies have also been recently employed to redefine the tropism of AAV vectors.[18–21] These single-domain antibodies are particularly attractive due to their small size, stability, specificity, and high affinity for the target receptor.[22]

We aimed to retarget AAV2 to tumor cells and tissues expressing the fibroblast activation protein (FAP) receptor. FAP receptor is a type II integral membrane protein distinctly upregulated in the tumor stroma and the stroma of fibrotic tissues, but expression is rare or low in normal and healthy tissues.[23–27] Hence, targeting FAP receptor offers a robust and elegant opportunity to deliver cancer therapies to the stromal fibroblast of the tumor microenvironment (TME) in a broad variety of epithelial cancers with high degree of specificity.[26–29] Our colleagues recently developed the first antibody AAV-based platform for the specific targeting of FAP receptor-expressing cells.[30] This was achieved by utilizing a bispecific antibody that recognizes a short linear 2E3 epitope engineered on the capsid surface as well as the FAP receptor on FAP-expressing cells, the AAV was functionalized for targeting FAP-expressing cells *in vitro*.[30]

In this study, we functionalized the capsid surface of AAV2 by genetically incorporating an anti-FAP nanobody (αFAP_Nb or VHH) on

Received 11 July 2024; accepted 8 November 2024;
https://doi.org/10.1016/j.omtm.2024.101378.

Correspondence: Francois du Plessis, AAV Gene Therapy Research Group, Research Beyond Borders (RBB), Boehringer Ingelheim Pharma GmbH & Co. KG, 88400 Biberach an der Riß, Germany.
E-mail: francois.du_plessis@boehringer-ingelheim.com

the GH2/GH3-exposed loop of VP1, thereby strongly mediating the retargeting of the vector specifically to FAP receptor-expressing tumor cells and tissues. To limit the copies of αFAP_Nb per capsid to not more than five copies, the sequence of αFAP_Nb was integrated on the GH2/GH3 loop of VP1 and the modified VP1 was expressed from a pCMV-VP1-αFAP-Nb plasmid during AAV packaging. Following multiple rounds of rational design and optimization of the VP1 capsid cassette, the transduction efficiency of the retargeted AAV2 vectors were improved to levels comparable with or higher than unmodified AAV2 vector, while maintaining high specificity for the target cells. Depending on the promoter used to drive the expression of the αFAP_Nb-VP1 during AAV packaging, we observed distinct differences in the incorporation efficiency of the αFAP_Nb containing VP1 in the capsid, as well as the overall transduction efficiency of the retargeted AAV2 vectors. In addition, we further expanded the robustness and versatility of the platform by performing a VHH antibody discovery campaign using a naive yeast display library to identify novel αFAP nanobodies for the subsequent functionalization of the AAV capsid. We identified and characterized several αFAP nanobodies with binding affinities to FAP ranging between 0.1 and >100 nM.

In summary, our data show the potential for a highly selective and specific retargeting of AAV vectors to the tumor stroma. Utilizing iterative improvements in rational capsid engineering, this study enables the advancement of targeted delivery of gene therapies not just to tumors, but any cell or tissue type of interest.

RESULTS

Genetic incorporation and the concomitant productivity analysis of αFAP VHH (αFAP_Nb) in the VP1 of AAV2 VP1

To design and generate AAV particles exhibiting high tropism toward FAP receptor-expressing neoplastic cells, an αFAP_Nb was incorporated within the variable region IV (VR-IV) that harbors the GH2/GH3 loop. Specifically, the nanobody, comprising 126 amino acids, was integrated at the G453-R459 amino acid position on the capsid, an approach that aligns with earlier strategies for the insertion of large scaffolds into the GH2/GH3 surface loop, a region common to VP1, VP2, and VP3.[18–20,31] To display up to 5 αFAP_Nb copies per capsid, the native VP1 start codon was mutated on the AAV2 *Rep/Cap* plasmid thereby inhibiting the expression of VP1 from its inherent configuration. Subsequently, the αFAP_Nb, flanked by a flexible short GGGS linker at both the N- and C-terminal ends, was incorporated into the GH2/GH3 loop of the VP1 protein, where the VP2 and VP3 start codons were mutated to suppress the expression of VP2 and VP3, respectively. To ensure this conformation, the αFAP_Nb-containing VP1 was supplied in *trans* on a second plasmid under the control of a CMV promoter, thereby resulting in a four-plasmid transfection to enable rAAV packaging (Figure 1A). Moreover, the heparan sulfate proteoglycans (HSPGs) receptor binding motifs contained in the capsid backbones of both the modified VP1 and the native VP2/VP3 were mutated by replacing the arginine residues at positions 585 and 588 with alanine, thereby negating background or residual targeting to the primary and native AAV2 HSPG binding motif.[19,32,33] Recombinant AAV particles displaying the αFAP_Nb and harboring a transgene cassette encoding for a nanoluciferase (NanoLuc) protein (AAV-αFAP_Nb) were assembled and produced in HEK293 cells. The packaging efficiency was evaluated using digital PCR (dPCR) to ascertain the titer and yield per cm^2 of cell disc, and western blot was performed to characterize the capsid proteins composition of the modified AAVs. Comparing the yield of the αFAP_Nb displaying vector with that of unmodified AAV2, an estimated 15-fold decrease in yield was observed per cm^2 (Figure 1B).

Earlier studies underscored the difficulties associated with the production of modified AAV capsids, which display cysteine residue-containing targeting ligands. These challenges are due to the reducing conditions in the nucleus, which is not optimal for antibody processing and folding; a phenomenon that requires an oxidizing environment.[13,34] As a control, a long 42 amino acid peptide devoid of cysteine residues was integrated in the same loop as the nanobody, resulting in the generation of recombinant AAV2-Pep particles. The yield of AAV2-PEP was 6-fold lower than that of AAV2 (Figure 1B).

We characterized the expression of VP1 via western blot analysis using a monoclonal B1 antibody (PROGEN) that simultaneously detects VP1, VP2, and VP3. The incorporation of VP1-αFAP_Nb subunit into AAV-αFAP_Nb was detected; however, the efficiency was significantly lower relative to VP2, whereas in AAV2 the amounts of VP1 and VP2 are similar (Figure 1C). To further increase the sensitivity, a VP1/VP2 specific antibody (PROGEN) was used to probe for VP1 and VP2 expression, confirming the successful assembly of the VP1-fused nanobody in the AAV-αFAP_Nb capsid (Figure 1D). Biophysical characterizations of AAV-αFAP_Nb were performed to determine particle size and aggregation, and we observed no distinct differences in the aggregation profile of AAV-αFAP_Nb in comparison with that of the parental AAV2 serotype (Figure 1E). However, thermal stability analysis shows an average of +2°C increase in the onset of melting of AAV-αFAP_Nb compared with AAV2 (Figure S1B). Overall, we observed a +1°C increase in the melting temperature of AAV-αFAP_Nb (Figure S1B).

Display of the αFAP_Nb on the capsid surface alters vector tropism and facilitates selective *in vitro* transduction of human FAP receptor-expressing HT1080 cells

The targeting potential and transduction efficiency of AAV-αFAP_Nb was assessed in a genetically modified human fibrosarcoma HT1080 cell line that stably expresses the human FAP receptor (HT1080-huFAP), while the non-FAP receptor-expressing counterpart (HT1080-Neo) served as a negative control. The cells were transduced with a multiplicity of infection (MOI) of 1×10^4 vector genome per cell (VG/cell) with either AAV2, AAV2 with HSPG ablated (AAV2-KO), or AAV-αFAP_Nb. Following transduction, the cells were analyzed for NanoLuc expression after 72 h using a luminescence plate reader. We noted that AAV-αFAP_Nb selectively and efficiently transduced HT1080-huFAP cells, with a 33.6-fold increase over the negative control HT1080-Neo cells. Conversely, as anticipated, the HSPG-ablated AAV2-KO poorly transduced both cell lines serving as background control (Figure 2A). Dose-dependent transduction of AAV-αFAP_Nb using MOIs between 1.0E+01 to 1.0+E05 VG/cell shows similar selective

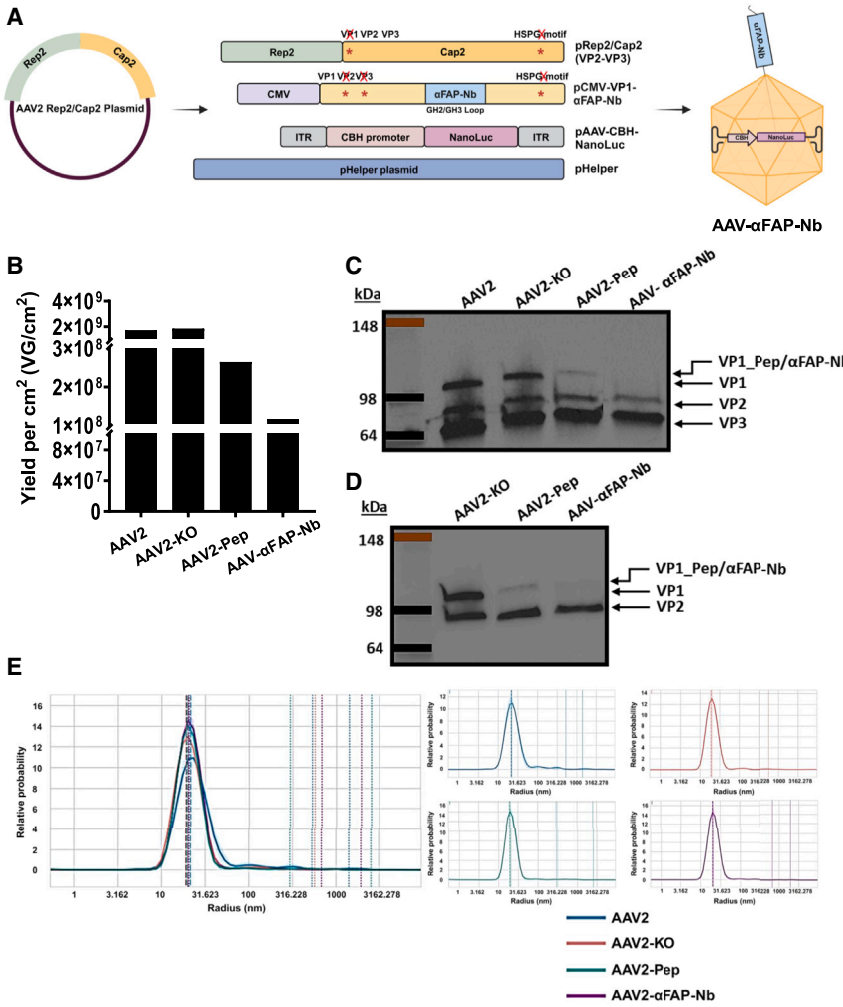

Figure 1. Genetic incorporation of human αFAP_Nb in AAV2 VP1 and biophysical characterization of AAV-αFAP_Nb

(A) Overview of the capsid engineering strategies showing modifications to the viral capsid proteins. The human αFAP_VHH was integrated in the GH2/GH3 loop of VP1 under the control of a CMV promoter and native HSPG receptor-binding motifs were ablated. Recombinant AAVs were packaged using four plasmid transfection and the modified VP1 cassette was supplied in *trans*. (B) Evaluation of the productivity of the modified AAVs in comparison with AAV2 vector with wild-type capsid and the HSPG-ablated capsid variant. (C) Western blot analyses of the VP1, VP2, and VP3 capsid proteins composition using the monoclonal anti-VP1/VP2/VP3 B1 monoclonal antibody. (D) VP1, VP2 capsid protein analysis using anti-VP1/VP2 A69 monoclonal antibody. (E) Comparative characterization of the particle sizes of AAV2 vector and the modified capsid variants.

transduction of HT1080-huFAP cells (Figure S2B). The αFAP_Nb displayed on the AAV capsid is specific for the human FAP receptor. We therefore assessed whether the human FAP-targeting capsid could selectively transduce mouse FAP receptor-expressing HT1080 cells (HT1080-muFAP). As expected, no selective transduction of HT1080-muFAP cells was observed (Figure 2B), corroborating the specificity of AAV-αFAP_Nb for its target cells. To further test for off-target of AAV-αFAP_Nb, the capsid was incubated with HEK293T cells, which inherently do not express the FAP receptor (Figure S2B). We showed that AAV-αFAP_Nb was also incapable of transducing HEK293T cells (Figure 2C). This demonstrates that the observed transduction of AAV-αFAP_Nb in HT1080-huFAP cells is heavily reliant on the interaction between the αFAP_Nb and the human FAP receptor present on the HT1080-huFAP cells.

To determine whether the modified αFAP_Nb-presenting vector directly and specifically interacts with the target human FAP receptor on HT1080-huFAP cells, a series of competitive inhibition assays were conducted. Utilizing two anti-FAP monoclonal antibodies (αFAP-mABs) with different binding affinities to FAP, as well as a soluble FAP extracellular domain (ECD). We observed potent inhibition of AAV-αFAP_Nb's ability to transduce HT1080-huFAP cells (Figures 2D–2F), verifying the specificity and direct interaction of the vector with the FAP receptor via the integrated αFAP_Nb.

AAV-αFAP_Nb demonstrates a highly specific and significantly enhanced transduction of human FAP-expressing tumor tissues *in vivo*

To evaluate the suitability of AAV-αFAP_Nb for selective gene delivery to target tissues *in vivo*, two distinct models of HT1080-huFAP cell-derived xenograft tumor models were generated using the immunodeficient NXG (NOD-Prkdc^{scid}-IL2rg^{Tm}1/Rj) mouse strain. In one model, the tumor cells were implanted in the mammary fat pad and, in the other, the tumor was subcutaneously implanted. Thereafter, 1×10^{11} VG of either the FAP-targeted AAV or AAV2 was administered intravenously. Interestingly, for the mammary fat pad tumor group, *in vivo* bioluminescence imaging shows an early onset of NanoLuc activity, already discernible at 24 h post AAV-administration, with the most pronounced bioluminescence signals observed in the tumors of mice administered with the human FAP-targeting AAV-αFAP_Nb vector. The luminescence signal increased further up to day 7 following the AAV administration with a distinct localization to the tumor-bearing area (Figure 3A). For the AAV2-administered mice, however, high NanoLuc activity was observed in the liver region with diffuse luminescence observed in the tumor tissues. *Ex vivo* bioluminescence imaging was conducted on collected tissues, which included the liver, tumor, lung, heart, and spleen. Overall, a 10-fold lower luminescence activity was observed

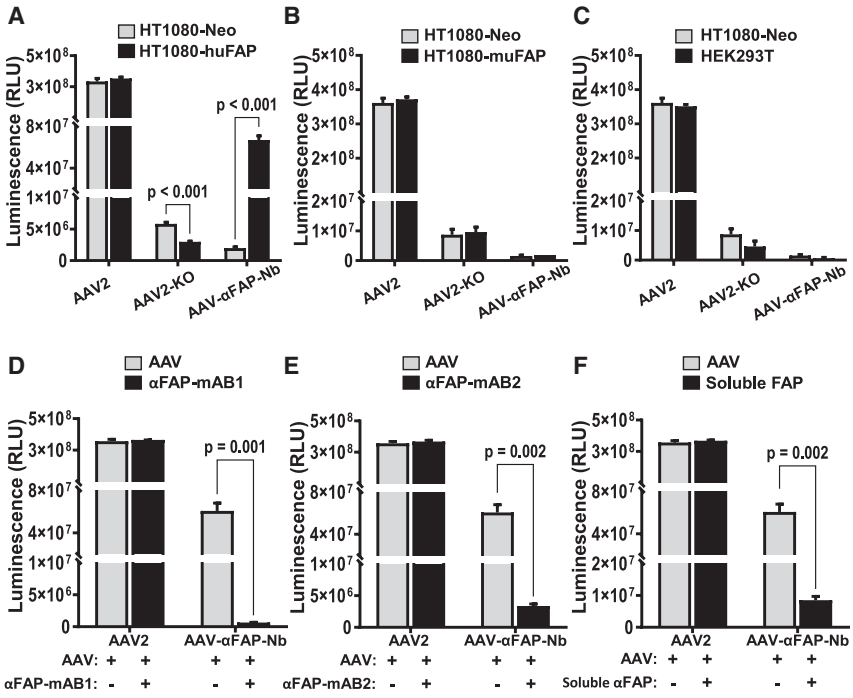

Figure 2. Display of αFAP_Nb on AAV capsid surface mediates retargeting of the capsids to human FAP-expressing cells

(A) Human HT1080 cells expressing either the human FAP receptor (HT1080-huFAP) or the negative control (HT1080-Neo) were incubated with 1×10^4 VG/cells of the indicated AAV vectors expressing NanoLuc transgene. NanoLuc protein expression was determined and quantified 72 h after incubation. Off-target analyses of the modified AAV-αFAP_Nb in (B) human HT1080 cells expressing the mouse FAP receptor (HT1080-muFAP) and (C) in non-FAP receptor expressing HEK293T cells. Competitive inhibition of AAV-αFAP_Nb by in-house-generated αFAP-mAB1 (D), αFAP-mAB2 (E), and soluble FAP protein (F). The values shown represent three independent experiments. Error bars are presented as ± SEM of the three independent experiments. *p* value was determined by two-tailed Student's t test. $^*p < 0.05$, $^{**}p < 0.01$, $^{***}p < 0.001$.

in the liver tissues isolated from AAV-αFAP_Nb-administered mice compared with that of AAV2 mice and a 6.4-fold increase in the luminescence signals in the tumor tissues of AAV-αFAP_Nb mice compared with AAV2 mice. (Figures 3B and 3C). Generally, low luminescence signal was observed in the spleen (Figure 3C), lung, and heart tissues of both AAV2-treated mice and AAV-αFAP_Nb-treated mice (Figure S3A). Subsequently, vector DNA biodistribution was analyzed by quantifying the vector genomes retrieved from the tissues. Consistent with the *ex vivo* bioluminescence signal data, the AAV-αFAP_Nb vector was strongly detargeted (8.8-fold) from the liver and (19.2-fold) from the spleen, with increased accumulation (5.5-fold) of the vector in the tumor tissues (Figure 3D). Finally, NanoLuc mRNA expression was quantified to further correlate the vector DNA biodistribution data with mRNA expression. NanoLuc mRNA was completely abrogated in the AAV-αFAP_Nb liver tissues, while expression was significantly increased in the tumor tissues (Figure 3E). Interestingly, despite the disproportionately high AAV2 vector genome accumulation in the spleen, NanoLuc mRNA expression was almost non-existent, suggesting high clearance of the vector genomes from the spleen (Figure 3E).

For the second tumor model, HT1080-huFAP cells were subcutaneously engrafted in one flank of the NXG (NOD-Prkdc^{scid}-IL2rg^{Tm}1/Rj) mouse strain, whereafter 1×10^{11} VG of either AAV2 or AAV-αFAP_Nb harboring NanoLuc were administered. We obtained similar results, highly comparable with the mammary fat pad model. The FAP-targeting vector was detargeted from the liver, spleen, and we observed strong and selective tumor targeting and transduction (Figure S4). Although, the quantity of vector genomes in the lung and heart tissues for both AAV2 and AAV-αFAP_Nb were similar, lower luminescence signal was observed in the AAV-αFAP_Nb group (Figure S5). Overall, in both tumor models, we demonstrated high and selective tumor-targeting potentials of the AAV-αFAP_Nb vector.

Incorporation of αFAP_Nb-containing VP1 during capsid assembly is promoter dependent and plays a role in enhancing transduction

Despite the significant on-target efficacy (23- to 80-fold) and the exceptional selective transduction of the target HT1080-huFAP cells by the FAP-targeting AAV-αFAP_Nb vector, we noticed that the transduction efficiency was 5-fold lower than that of AAV2 (Figure 2A). We postulated that this discrepancy might be attributable to the low incorporation of the CMV promoter-driven αFAP_Nb-VP1 species during the capsid assembly process. The CMV promoter is frequently subjected to epigenetic alterations such as DNA methylation, histone deacetylation, and histone methylation in some cell types.[35–37] Consequently, the CMV promoter was replaced by the EF1α promoter to drive the expression of αFAP_Nb-VP1 species during AAV packaging resulting in a version of the capsid termed "AAV-αFAP_Nb2" (Figure 4A). Western blot analyses of the AAV-αFAP_Nb2 capsid confirmed an increase in the incorporation of αFAP_Nb-VP1 in the capsid compared with AAV-αFAP_Nb (Figures 4B and 4C). Subsequently, the transduction efficiency and on-target specificity of AAV-αFAP_Nb2 were evaluated. Transduction efficiency was markedly amplified to levels close to AAV2 while preserving high specificity and selectivity (on-target score = 22-fold) for human FAP receptor-expressing HT1080-huFAP cells (Figure 4D). Profiling for off-target transduction of

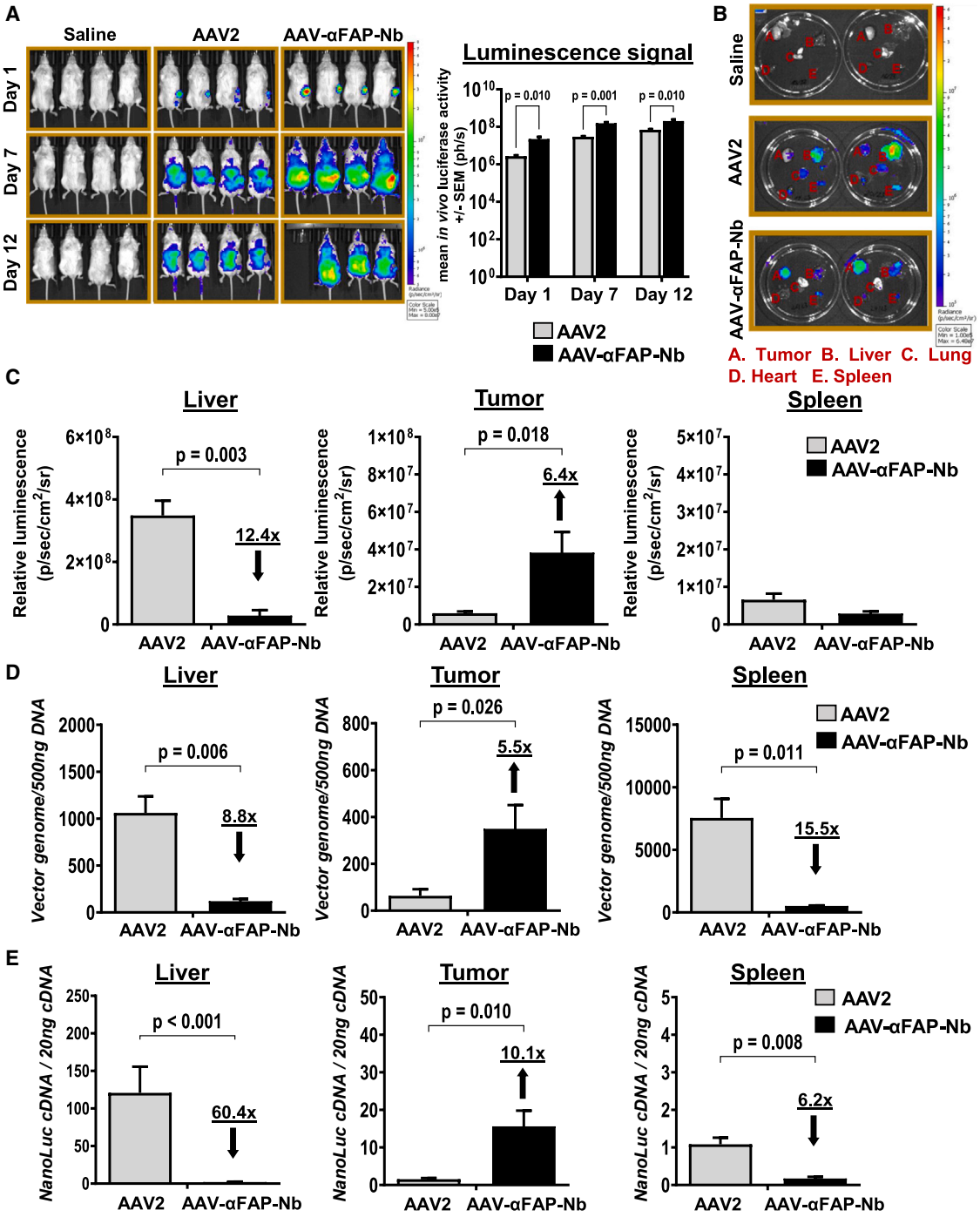

Figure 3. αFAP_Nb mediates successful retargeting of AAVs to HT1080-huFAP tumors *in vivo*

(A) HT1080-huFAP tumors were engrafted in the mammary fat pad of immunodeficient NXG mouse strain. After tumor volume of 30–60 mm^3 was attained, 1×10^{11} VG of either AAV2 or the retargeted AAV-αFAP_Nb vector was administered intravenously per mouse. *In vivo* bioluminescence imaging was performed to detect nanoluciferase activity at day 1, day 7, and day 12 post-AAV administration and the corresponding plot of the average luminescence signal. (B) *Ex vivo* bioluminescence imaging of the nanoluciferase activity in the liver, tumor, lung, heart, and spleen tissues collected after termination of the experiment. (C) Quantification and comparison of the nanoluciferase activity in tissues collected from AAV2 mice and AAV-αFAP_Nb mice. (D) Analysis and comparison of the biodistribution of AAV2 and AAV-αFAP_Nb vector genomes in tissues retrieved from the HT1080-huFAP cell-derived xenograft mice. (E) Quantification of NanoLuc mRNA expression levels in the collected tissues. Data are presented as ± SEM for $n = 3$–4 mice. p value was determined by two-tailed Student's t test. $^*p < 0.05$, $^{**}p < 0.01$, $^{***}p < 0.001$.

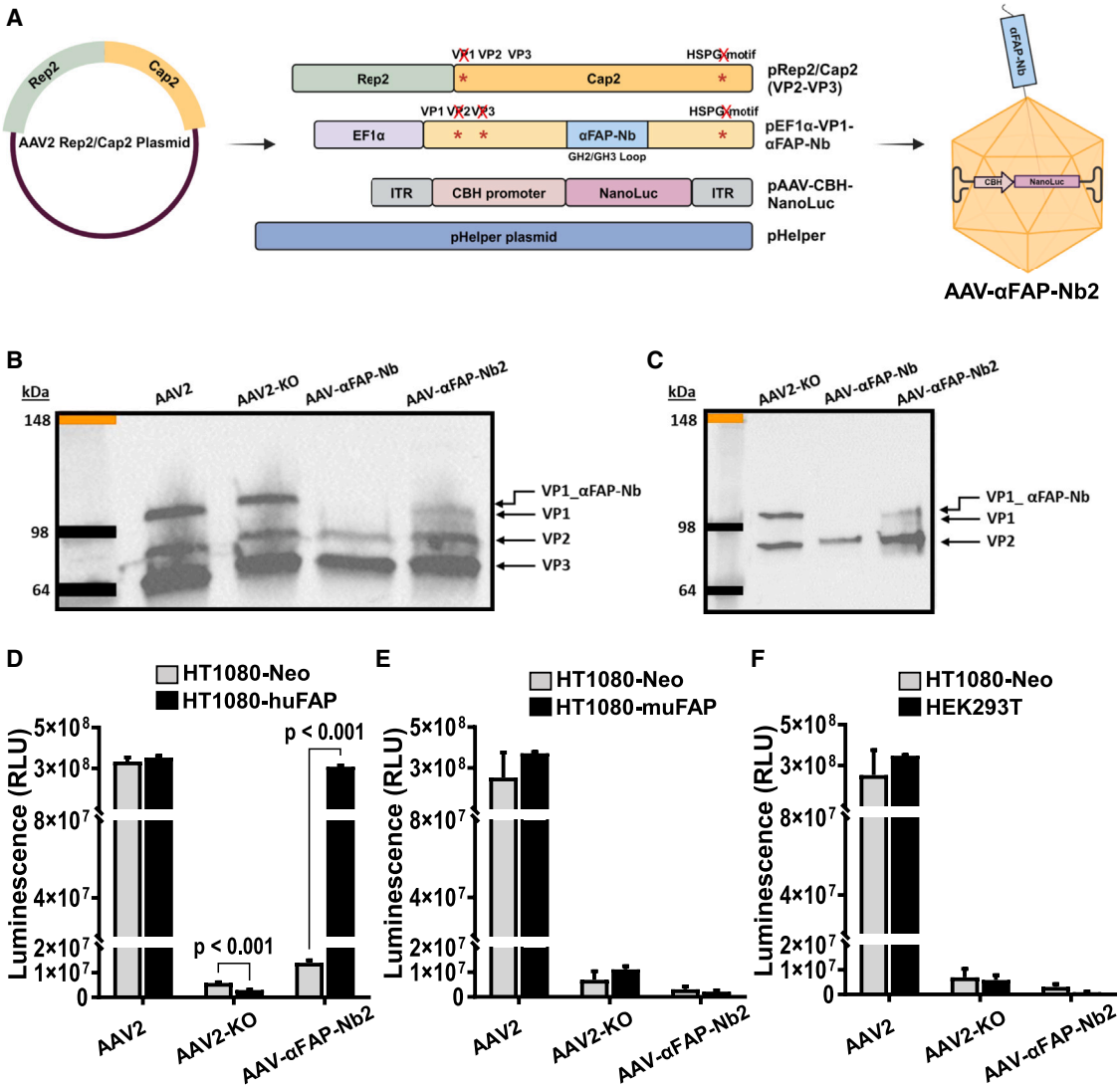

Figure 4. Incorporation of modified VP1-αFAP_Nb during AAV packaging is promoter dependent

(A) Schematics of the substitution of CMV promoter with an EF1α promoter for driving the expression of the modified VP1-αFAP_Nb expression cassette during AAV packaging and generation of AAV-αFAP_Nb2 vector. (B) Western blot analyses of the VP1, VP2, and VP3 capsid proteins composition using the monoclonal anti-VP1/VP2/VP3 B1 monoclonal antibody. (C) VP1, VP2 capsid protein analysis using anti-VP1/VP2 A69 monoclonal antibody. (D) Determination of the transduction efficiency AAV-αFAP_Nb2 in HT1080-huFAP cells and the off-target analyses of the improved vector in (E) human HT1080-muFAP cells, as well as (F) in HEK293T cells. The values shown represent three independent experiments. Error bars are presented as ± SEM of the three independent experiments. *p* value was determined by two-tailed Student's t test. $^{*}p < 0.05$, $^{**}p < 0.01$, $^{***}p < 0.001$.

HT1080-muFAP and HEK293T cells revealed no off-targeting to either cell line (Figures 4E and 4F). Analogous to the AAV-αFAP_Nb vector, competitive inhibition of AAV-αFAP_Nb2 with αFAP-mABs and soluble FAP ECD disrupted surface-displayed ligand-target engagement. This consequently inhibited transduction, thus corroborating the observed transduction was facilitated by the direct interaction of the αFAP_Nb with the target FAP receptor on HT1080-huFAP cells (Figures S6A–S6C).

Optimization of the αFAP_Nb VP1 expression cassette design further enhances transduction efficiency

In an auxiliary strategy to refine the design of the FAP-targeting AAV vector and maximize its transduction efficiency, we further "decorated" the capsid with a nuclear localization signal (NLS) to enhance the translocation of the capsid to the nucleus following αFAP_Nb-mediated cellular uptake. To facilitate this, a formerly delineated c-myc NLS[38] encoding sequence was fused either at the 3′ or 5′ terminus of the αFAP_Nb DNA sequence in VP1 separated by a GGGS

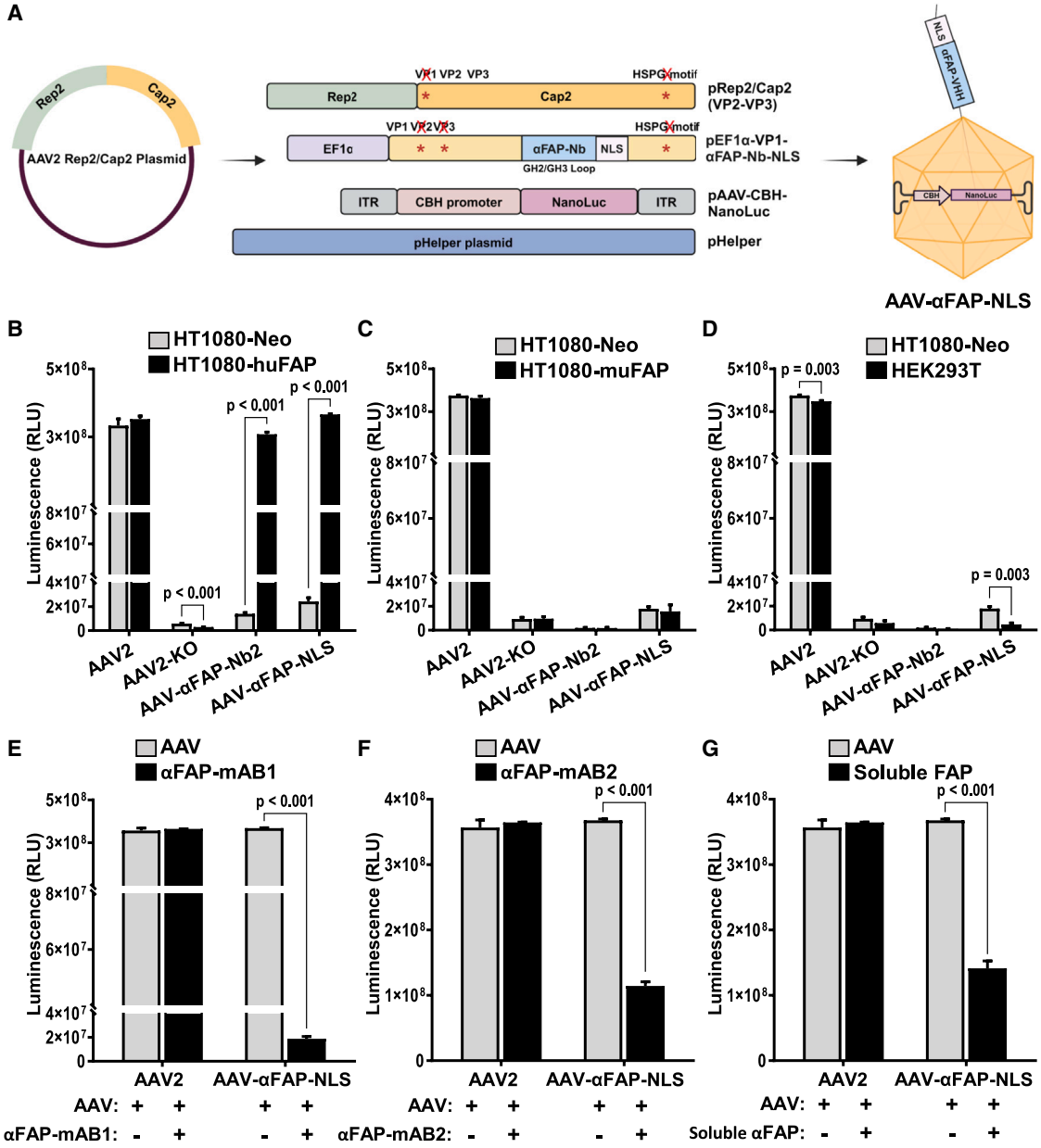

Figure 5. Further optimization of the VP1-αFAP_Nb expression cassette with an NLS enhances transduction efficiency

(A) Schematics of the capsid engineering strategy showing the introduction of an NLS sequence at the 3′ end of the αFAP_Nb on VP1 and generation of AAV-αFAP_**NLS** vector. (B) *In vitro* validation of the transduction efficiency of the optimized AAV-αFAP_**NLS** in HT1080-huFAP cells and the subsequent off-target analyses in HT1080-muFAP cells (C), as well as in HEK293T cells (D). Competitive inhibition of AAV-αFAP_**NLS** by in-house-generated αFAP-mAB1 (E), αFAP-mAB2 (F), and soluble FAP protein (G). The cells were transduced with MOI of 1×10^4 VG/cell and cells were analyzed for luminescence expression at 72 h post-transduction. The values shown represent three independent experiments. Error bars are presented as ± SEM of the three independent experiments. *p* value was determined by two-tailed Student's t test. $^*p < 0.05$, $^{**}p < 0.01$, $^{***}p < 0.001$.

linker (Figures 5A and S7A). The expression of the VP1 αFAP_Nb NLS fusion cassettes was driven by an EF1α promoter during AAV packaging, and we generated AAV-αFAP-**NLS**_Nb2 and AAV-**NLS**-αFAP_Nb2 vectors with the NLS sequence flanking the αFAP_Nb either at the 3′ or 5′ end, respectively. Results from the transduction of the NLS αFAP_Nb displaying vectors showed that fusing the NLS at the 3′ end of αFAP_Nb improved the transduction efficiency of the vector modestly by ∼20% (Figure 5B), while fusion at the 5′ end improved the transduction efficiency of the vector by ∼10% (Figure S7B). Collectively and premised on these optimizations, the

Table 1. Measurements from SPR kinetics and affinity analysis

	Human FAP			Mouse FAP			Cynomolgus FAP		
Name	K_a (1/Ms)	K_d (1/s)	K_D (M)	K_a (1/Ms)	K_d (1/s)	K_D (M)	K_a (1/Ms)	K_d (1/s)	K_D (M)
Nb-1610	1.2E+06	1.1E−04	9.2E−11	1.2E+06	6.6E−04	5.5E−10	1.3E+06	1.4E−04	1.1E−10
Nb-1611	1.3E+06	4.6E−03	3.5E−09	no binding at 100 nM			1.5E+06	5.1E−03	3.4E−09
Nb-1612	no binding at 100 nM			no binding at 100 nM			no binding at 100 nM		

k_a, association rate constant; k_d, dissociation rate constant; K_D, dissociation equilibrium.

transduction efficiency of the human FAP-targeting AAV was augmented to align with that of AAV2 (Figures 5B and S7B). However, while a high on-target efficiency and selectivity for the HT1080-huFAP cells (15- to 18-fold) was preserved, a slight increase in the basal transduction of the off-target cell lines—HT1080-Neo, HT1080-muFAP, and HEK293T cells—was observed (Figures 5B–5D, S7C, and S7D). This can be ascribed to the non-specificity of the NLS targeting, especially since only the αFAP_Nb confers specificity, and not NLS. This was further corroborated by elevated background transduction levels observed when vectors AAV-αFAP-**NLS**_Nb2 (Figures 5E–5G) and AAV-**NLS**-αFAP_Nb2 (Figures S7E–S7G) were competitively inhibited with αFAP-mABs and soluble FAP ECD. Consequently, it is imperative to note that further modifying the targeting ligand-containing VP1 cassette with an NLS brought a marginal increase in transduction efficiency and a disadvantage of potential increase in the transduction of off-target tissues.

Functionalization of AAV capsid for FAP tumor targeting with novel αFAP nanobodies identified from naive VHH yeast display

To augment the versatility of our high-fidelity nanobody-based targeting platform and tackle the limitations presented by the limited availability of nanobody repertoires, we utilized an *in vitro* antibody discovery platform, naive VHH yeast display, to identify novel VHH candidates for subsequent AAV capsid functionalization. We successfully identified and characterized several novel human α-FAP nanobody candidates with binding affinities to FAP ranging between K_D = 0.1 to >100 nM and with cross-reactivity to the human and cynomolgus versions of FAP (Table 1). Three candidates—Nb-1610 (K_D = 0.09 nM), Nb-1611 (K_D = 3.5 nM), and Nb-1612 (K_D >100 nM) —were chosen for the initial capsid functionalization predicated on their binding affinities for FAP, which we classified as high, medium, and weak binders. While Nb-1611 and Nb-1612 exhibited no cross-reactivity with muFAP, the high-affinity binder Nb-1610 cross-reacted with muFAP in the sub-nanomolar range (Table 1). These three novel αFAP nanobodies were subsequently incorporated in the GH2/GH3 loop of AAV2's VP1, and the EF1α promoter was employed to drive the expression of the VP1 cassette during AAV packaging as described previously for AAV-αFAP_Nb2 in Figure 4A. The generated AAV particles AAV-Nb1610, AAV-Nb1611, and AAV-Nb1612 were characterized *in vitro* for their ability to target FAP receptor-expressing cells and compared with those of AAV-αFAP_Nb2. The result indicates the transduction efficiency and specificity of the single-digit binder AAV-Nb1611 are comparable with that of AAV-αFAP_Nb2, where αFAP-Nb displayed on the capsid has a binding affinity of K_D = 30 nM. The transduction efficiency of the high-affinity binder AAV-Nb1610 was significantly lower while the weak binder AAV-Nb1612 did not mediate the transduction of the target cells (Figure 6A). Our observations correspond to those observed in the antibody internalization field where very-high- and very-low-affinity IgGs internalize weakly and the optimal affinities for

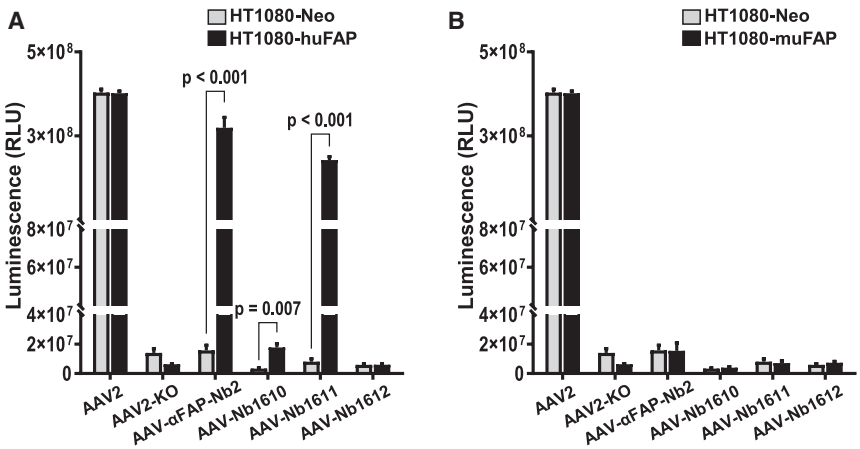

Figure 6. Functionalization of the AAV capsid with novel αFAP VHHs identified in a naive VHH yeast display screening

(A) Three novel αFAP VHHs Nb-1610, Nb1611, and Nb-1612 identified from our in-house naive VHH yeast display library screen, were integrated in the AAV capsid as previously shown in Figure 4A. The transduction efficiencies of the novel VHHs displaying AAVs were functionally validated *in vitro* for HT1080-huFAP cells targeting and compared with that of AAV-αFAP_Nb2. (B) Determination of the transduction efficiencies of the indicated AAVs HT1080-muFAP cells. The cells were transduced with MOI of 1 × 10^4 VG/cell and cells were analyzed for luminescence expression at 72 h post-transduction. The values shown represent three independent experiments. Error bars are presented as ± SEM of the three independent experiments. *p* value was determined by two-tailed Student's t test. **p* < 0.05, ***p* < 0.01, ****p* < 0.001.

internalization fall between single-digit to low-double-digit nanomolar range.

Subsequently, we evaluated if the newly generated FAP receptor-targeting AAV-Nb1611 off-targets to muFAP and ascertained if the high-affinity binder AAV-Nb1610 could potentially transduce muFAP, since it displayed the Nb-1610 nanobody that cross-reacts with muFAP (K_D = 0.55 nM). The transduction efficiency of the AAV vectors was determined in HT1080-muFAP cells. As expected for the AAV-Nb1611 vector, the result shows that this AAV does not transduce muFAP. Interestingly, the same phenomenon was observed for the high-affinity binder AAV-Nb1610 (Figure 6B), showing that it did not transduce muFAP-expressing cells. Finally, we evaluated the off-target potentials of the vectors in HEK293T cells that do not express FAP receptor. AAV-Nb1611 again maintained a similar off-target profile to AAV-αFAP_Nb2 (Figure S8). In summary, a novel single-digit nanomolar binder Nb-1611 identified from our in-house yeast display VHH library campaign demonstrated a comparable targeting profile with that of the previously validated αFAP_Nb when used as a targeting ligand for capsid functionalization. In the future, additional candidates from our screening campaign will be evaluated with strong focus on identifying binders that simultaneously cross-react with mouse, human, and cynomolgus FAP for subsequent AAV capsid functionalization.

DISCUSSION

Leveraging AAVs as agents for the selective delivery of therapeutic agents to the tumor environment remains an attractive, albeit insufficiently investigated strategy for gene immuno-oncotherapy applications. Anti-tumor interventions such as immunotherapies and antibody-drug conjugates have demonstrated high efficacy as therapeutic measures to address the high unmet need in the cancer therapy landscape.[39–41] However, the consequential dose-limiting cytotoxicity, extended plasma circulating half-life, and off-target profile ensuing from systemic administration present formidable limitations to the success of these comparatively novel cancer therapeutic modalities. Therefore, the development of delivery mechanisms, such as highly specialized AAV vectors, for the targeted delivery and expression of these anti-cancer agents selectively within the neoplastic microenvironment, could provide a versatile toolset for a more extensive adoption of these therapeutic modalities in the clinic.[42,43] Here, we report a proof-of-concept study showing that a genetically modified AAV2 capsid can be specifically retargeted to tumor tissues expressing a tumor-specific receptor.

FAP is uniquely expressed on the cell surface of reactive stromal fibroblasts, such as cancer-associated fibroblasts (CAFs) found in the TME and other disease states such as fibrosis.[44–46] While FAP is also expressed in granulation tissues during wound repair and basal level expression exists in some tissues, the protein is more distinctly elevated in reactive stroma fibroblasts, such as CAFs.[47,48] Although the mechanism remains somewhat enigmatic, FAP has been directly implicated in promoting classical hallmarks of cancer.[45] This includes driving cell proliferation, differentiation, migration, and invasiveness, as well as playing roles in immune regulation and angiogenesis. Consequently, therapeutic targeting of FAP presents promising opportunities either to directly target the protein within the TME, with the objective of depleting FAP^+ cells, thereby eradicating the supportive roles they play in maintaining the tumor stroma,[29,45,49,50] or alternatively to exploit FAP-expressing CAFs as a localized, stroma-based factory for the bioproduction of anti-tumor agents directly into the tumor stroma.[51] Therefore, strategically redirecting AAVs to utilize the FAP receptor as an attachment factor to mediate the selective uptake of the vectors into the TME, could offer a robust approach to reach the tumor stroma.

Kuklik et al. have previously showcased the versatility of this concept by retargeting a "blinded" 2E3 epitope displaying AAV2 vector to engage the FAP receptor.[30] This approach was predicated on a non-covalent linkage technology, mediated by a bispecific antibody (bsAb). This antibody recognizes and attaches to the 2E3 epitope engineered on the capsid surface with one arm, while the other arm of the antibody selectively bound the FAP receptor. *In vitro* data indicated that the resulting AAV particles, which bound bsAbs on the capsid surface, were successfully retargeted to FAP-expressing cells.[30] However, this approach would present difficulties when adapting for *in vivo* applications, particularly concerning the conjugation efficiency of the bsAbs to the capsids, the downstream purification strategy to enrich for AAVs displaying the bsAbs, and the stability of the capsid/bsAbs linkage in the patient's circulation following administration. Recently, Hartmann et al. reported their strategy to generate FAP-targeting adenovirus vectors, which have been engineered to genetically display FAP-binding DARPin scaffolds for the selective targeting of FAP-expressing cells *in vitro* and *in vivo*.[51] While adenoviruses provide the opportunity to deliver larger therapeutic cargoes beyond the 4.7 kb limit of AAVs, the adenovirus platform requires improvements to overcome challenges associated with high immunogenicity, transient expression of the therapeutic payload, and off-target transduction.[52–54]

Using AAV rational design capsid engineering, we genetically anchored a FAP-specific αFAP VHH on VP1's GH2/3 loop of an HSPG-ablated AAV2 capsid surface to mediate the specific targeting of FAP-expressing cells and tumors. While the AAV particles displaying αFAP_Nb were successfully packaged in HEK293H cells using a four-plasmid transfection system, a considerable reduction of 15- to 20-fold in the packaging efficiency of the VP1 modified vector was observed compared to that of the AAV2. This phenomenon is consistent with the challenges associated with displaying cysteine-residue containing antibody species on the capsid during AAV assembly, as reported previously.[13,19,34,55] We performed in-depth biophysical characterization of the αFAP_Nb displaying AAV particles, we observed the integration of the nanobody on the capsid did not promote capsid aggregation. However, we noticed a slight increase in the capsid melting temperature by a modest 1°C in comparison with AAV2. Due to the high sensitivity of the dynamic light-scattering device (Prometheus Panta), a +1°C difference is significant, but this might have no biological impact on the capsid.

Nevertheless, it is quite important to profile nanobody's impact on overall capsid stability and aggregation. Functionally, we validated the nanobody-displaying AAV particles and showed that vector particles are transduction competent and mediate specific targeting of FAP receptor-expressing HT1080 human fibrosarcoma cells with less than 5% off-target transduction *in vitro*. In contrast to Eichhoff et al. who flanked the nanobodies in their study with a long 25 amino acid linker on the C terminus and a short 5 amino acid linker on the N terminus,[19] we utilized a short GGGS linker on both termini of the nanobody. However, future approaches should critically evaluate the effect of the linker length on targeting VHH presentation on the capsid surface, thereby evaluating if the linker length has any impact on capsid assembly.

In order to eliminate the need for a fourth plasmid encoding αFAP_Nb-VP1 during AAV packaging, we attempted to insert the nanobody directly in the GH2/3 loop common to both VP1, VP2, and VP3 on the native AAV2 *Rep/Cap* plasmid. However, this iteration failed to generate AAV particles, as vector genomes were not detected in the preparation (data not shown). This suggests that simultaneously incorporating the nanobody in all three capsid proteins increases steric hindrances and the complexity of the post-translational events which culminate in AAV assembly. Next, we exploited the marked amenability of VP2 N terminus for the integration of large targeting ligands.[13,34,55] The nanobody was fused to the N terminus of VP2 and the modified VP2 was expressed from a fourth plasmid under the control of a CMV promoter, while VP2 expression was suppressed in the native AAV2 *Rep/Cap* plasmid. We determined that the yield of the αFAP_Nb was 4.4-fold lower than that of AAV2, and 3.4- to 4.5-fold higher than VP1-modified vectors. Unfortunately, the VP2-modified αFAP_Nb particles were transduction incompetent in all the configurations we functionally tested (data not shown). Similar observation of a lack of transduction activity was reported by Eichhoff et al. following integration of nanobodies on the N terminus of VP2.[19] This observation could be caused by the improper presentation of the nanobody on the VP2 N terminus or by a lack of interaction between its paratope and the target epitope. A possible alternative strategy would be to insert the nanobody in the GH2/GH3 of VP2, instead of VP1 and supply the modified VP2 in *trans*.

Prior studies have shown the potential of selective delivery of therapeutics in target cells by nanobody-mediated retargeted AAV vectors, but these investigations were majorly limited to *in vitro* validation.[18,19,56] Our study gives the first insight on the *in vivo* targeting potentials of nanobody-displaying AAVs in two distinct tumor types—intramammary fat pad and subcutaneous engrafted tumor tissues. Initially, we evaluated the capability of the αFAP nanobody displaying vector, AAV-αFAP_Nb, to selectively target and transduce human FAP-expressing tumor tissues engrafted in the mammary fat pad. Compared with AAV2, the novel FAP receptor-targeting capsid, AAV-αFAP_Nb, notably targets and transduces the intramammary fat pad tumors with high specificity and low off-target effects. Luminescence expression analysis in tissues revealed that AAV-αFAP_Nb mediated a 6.4-fold higher expression level in tumor tissues compared with wild-type AAV2 and a 10-fold lower expression level in the liver. Next, we implanted the tumor subcutaneously to assess the specificity and precision of our vector targeting in a different location. Comparable results were obtained from the subcutaneous tumor tissues, where a 9-fold lower liver transduction and a 5.5-fold increase in tumor transduction was observed for AAV-αFAP_Nb compared with AAV2. *In vivo* validation in the two distinct tumor locations highlights the huge potentials of the translatability of the specificity and precision of our targeted AAV vector. Particularly noteworthy is the double-digit detargeting of AAV-αFAP_Nb from the spleen in both scenarios, which might result in a significantly lower immunogenicity.

We aimed to further refine the expression cassette of the nanobody-incorporated VP1 by replacing the promoter driving the expression of VP1 during AAV production. Initially, the modified VP1 expression cassette was driven by a CMV promoter. However, in another study, we observed that expression of a modified VP2 cassette under EF1α promoter led to higher incorporation of the modified VP2 in the capsid compared to the CMV promoter (data not shown). We postulated that this is potentially applicable to the modified VP1 capsids. Consequently, the CMV promoter was replaced with EF1α, thereby creating an improved version of the AAV-αFAP_Nb, referred to as AAV-αFAP_Nb2. Promoter substitution significantly enhanced the transduction efficiency of AAV-αFAP_Nb2 to levels comparable with that of AAV2 and approximately 5-fold higher than the transduction efficiency of the initial version, AAV-αFAP_Nb. The introduction of a c-Myc NLS,[38] to further augment nuclear targeting marginally increased transduction, and concurrently increased background transduction, which could potentially increase the off-target profile *in vivo*.

The inability of our αFAP_Nb to cross-react with mouse FAP was a bottleneck to the use of mouse FAP-expressing endogenous genetic mouse tumor models, therefore limiting our studies to human FAP-expressing cell-derived xenografts. To address this limitation, a high-throughput yeast display library screening was performed, and we identified a subset of novel human, mouse, and cynomolgus FAP binders. However, presentation of the Nb-1610—which cross-reacted with both human and mouse FAP in SPR binding assay—on the AAV capsid (AAV-Nb1610) failed to mediate transduction to neither the human nor the mouse FAP receptor-expressing cells. Nb-1610 is a picomolar FAP binder; therefore, we speculate that the nanobody is too strongly tethered to the FAP receptor, such that the capsids are not sequestered from the receptor for subsequent endocytosis. Alternatively, the paratope of the nanobody could be wrongly presented on the capsid surface, thereby not being able to facilitate an interaction with the target epitope on the cell surface receptor. As an outlook, more candidate FAP binders will be functionalized on the capsid surface in the future and validated for selective mouse FAP targeting.

Here, in addition to the previously described impact of genetic integration of nanobodies or antibody species on the yield of AAV

capsids, we further identified other key parameters that play a role in the establishment of a robust platform. These include binding affinity, placement, and epitope accessibility of the selected nanobodies, as well as potential CMC considerations such as capsid stability and biophysical characteristics. Overcoming and understanding these considerations are critical for the maturation of the nanobody-based AAV retargeting platform. As we were finalizing our manuscript draft, Hoffmann et al. reported in their study the successful functionalization of an AAV-DJ capsid with a FAP-targeting nanobody. Similar to our findings, they showed a nanobody-mediated selective transduction of FAP-expressing cells by the capsids, demonstrating adaptability of this approach with another AAV capsid variant.[56]

In conclusion, this study presents a significant next step toward the understanding and utilization of second-generation capsid engineered AAVs as a potent tool for highly targeted delivery of therapeutic agents to the tumor stroma. The application of this platform extends beyond tumor targeting to any cell type or disease state of interest, thereby addressing the challenges posed by AAV's broad tropism, which often necessitates high vector dose administration to achieve clinical efficacy.

MATERIALS AND METHODS

Cloning of capsid and expression cassettes

To enable the generation of an AAV2 capsid harboring the genetically incorporated antibody sequence, the AAV2 *CAP* gene in its native *Rep/Cap* plasmid was modified by mutating the VP1 start codon to leucine (Leu), followed by the introduction of a stop codon at position 6 to ablate VP1 expression, while still maintaining VP2 and VP3 capsid protein expression. The αFAP nanobody coding sequence was derived from peptide sequencing of the commercially obtained anti-CD3 × anti-FAP VHH bispecific antibody (cat. no. BIVHH-022, Creative Biolabs, Shirley, NY). The αFAP nanobody sequence was inserted in position G453-R459, flanked by a GGGS linker on both termini on a modified VP1-only plasmid, named pVP1-αFAP_Nb. To prevent the expression of native VP2 and VP3 capsid proteins from the VP1-αFAP_Nb expression cassette, VP2 and VP3 expression was mutated on VP1-αFAP_Nb plasmid as follows. VP2 start: T138K; VP3 start: M203L, as well as M211L and M235L to prevent the expression of truncated VP3 species. The modified VP1-αFAP_Nb was supplied in *trans* and expressed from either a pTWIST-CMV or pTWIST-EF1α plasmid backbone (TWIST, San Francisco, CA), under the control of either a CMV or an EF1α promoter, respectively. The sequences were synthesized and cloned in their respective expression plasmids at TWIST. Transgene expression plasmid pAAV-CBA-NanoLuc consists of the native AAV2 ITR sequences which flank a chicken β-actin (CBA) promoter, Kozak sequence, NanoLuc transgene, and sv40 poly(A) signal sequence. The transgene expression cassette was synthesized and cloned by GeneArt (Thermo Fisher Scientific, Waltham, MA).

Cell lines and cell culture

HT1080 cells (ATCC, Manassas, VA) engineered as described previously[57] to express the human version of the FAP receptor (HT1080-huFAP), mouse FAP (HT1080-muFAP), and the corresponding negative control cells (HT1080-neo) were kindly provided by our colleague, Dr. John Park. The cells were cultured in RPMI 1640 medium (Thermo Fisher Scientific) supplemented with 10%, v/v, fetal bovine serum (Thermo Fisher Scientific), 1× MEM Non-Essential Amino Acids Solution (100×) (Thermo Fisher Scientific), and 300 μg/mL Geneticin Selective Antibiotic (Thermo Fisher Scientific).[30,57] HEK293T cells (ATCC) were cultured in an antibiotic-free DMEM high glucose, GlutaMax (Thermo Fisher Scientific) supplemented with 10% FCS. The cell lines were all maintained at 37°C and 5% CO_2 in a humidified incubator.

Recombinant AAV production and downstream analysis

AAV vectors were packaged in HEK293H cells (Thermo Fisher Scientific), using a calcium phosphate-based four-plasmid transfection (AAV helper free system; Agilent Technologies, Santa Clara, CA). The four plasmids were transfected in a ratio of 1:1:1:1 and AAVs were packaged and purified as described previously.[30,58] The titers of the AAV preparations were analyzed by dPCR.

AAV titer determination

AAV vector genome was quantified using dPCR. Fifty microliters of AAV prep was used as starting material and the vector DNA was extracted according to the manufacturer's protocol using ViralXpress Nucleic Acid Extraction Kit (Merck Millipore, Burlington, MA). Following extraction, the vector DNA was diluted in a 10-step dilution and added to QIAcuity Probe PCR Master Mix (QIAGEN, Hilden, Germany) and 1× primer-probe mix for the detection of the AAV2 ITR (forward primer: GGAACCCCTAGTGATGGAGTT, reverse primer: CGGCCTCAGTGAGCGA, probe FAM-CACTCCC TCTCTGCGCGCTCG-MGB) (Sigma-Aldrich, Burlington, MA) according to the manufacturer's instruction. dPCR reaction was performed on a QIAcuity One dPCR device (QIAGEN).

Western blot

rAAV particles (1×10^{11}) were incubated at 95°C for 5 min with NuPAGE LDS sample buffer (Thermo Fisher Scientific). An SDS-PAGE run was performed after the 50 μL sample mixes were loaded in a Mini-PROTEAN TGX stain-free gel (Bio-Rad, Hercules, CA) and allowed to run at 200 V for 1 h in a Mini-PROTEAN Tetra Vertical Electrophoresis Cell (Bio-Rad). The samples were transferred to a membrane using a Trans-Blot Turbo Transfer Pack (Bio-Rad) and the Trans-Blot Turbo Transfer System (Bio-Rad). The membrane was blocked at room temperature (RT) for 1 h with 5.0% milk in Tris-buffered saline plus 0.1% Tween (TBS-T), followed by primary antibody incubation with either an anti-mouse B1 IgG1 monoclonal anti-VP1/VP2/VP3 antibody (Progen, Heidelberg, Germany) or an anti-mouse A69 monoclonal anti-VP1/VP2 antibody (Progen) diluted 1:1,000 in 5.0% milk in TBS-T overnight at 4°C. Next, the membrane was washed 3× in TBS-T followed by incubation for 1 h at RT with 1:3,000 dilution of a goat anti-mouse IgG1 (H+L) HRP secondary antibody (Bio-Rad) in 5% milk in TBS-T. The SuperSignalWest Pico PLUS chemiluminescence substrate (Thermo Fisher Scientific) was used to

detect chemiluminescent signals by the ChemiDoc MP Imaging System (Bio-Rad).

Diameter and stability measurements

AAV biophysical properties such as particle size, aggregation, and thermal stability were measured in a label-free single run using the Prometheus Panta device (Nanotemper, Munich, Germany). Approximately 10–15 μL of 1×10^{12} VG/mL AAV samples were loaded per capillary in triplicate, and the particle size and thermal stability properties of the vectors were collected and analyzed automatically by the software.

In vitro transduction and nanoluciferase assays

For *in vitro* transduction assays, 1×10^4 HT1080-neo, HT1080-huFAP, and HT1080-muFAP or 7.5×10^3 HEK293T cells were seeded per well in Nunc F96 MicroWell cell culture white plates (Thermo Fisher Scientific). Twenty-four hours after seeding, the cells were incubated with a MOI of 1×10^4 VG/cell of the respective rAAV particles that encode a nanoluciferase transgene. Seventy-two hours later, equal medium volumes of the reconstituted Nano-Glo Luciferase Assay reagent (Promega, Madison, WI) was added per well and allowed to incubate for 10 min. The nanoluminescence activity was measured by transferring the plates to a SpectraMax i3x MiniMax 300 Imaging Cytometer (Molecular Devices, Sunnyvale, CA). For competitive inhibition assays, cells were pre-incubated at 37°C and 5% CO_2 for 1 h in a humidified incubator with 5 μg of anti-FAP monoclonal antibodies (generated in-house) followed by rAAV transduction of the cells. In a second approach, rAAV particles were pre-incubated at 4°C with an in-house generated soluble FAP protein for 1 h, followed by the addition of the pre-incubated AAV/soluble FAP protein to the cells. The cells were then analyzed 72 h after transduction for nanoluciferase expression.

In vivo xenograft studies

HT1080-huFAP tumor cells (5×10^6) in 100 μL Dulbecco's phosphate-buffered saline (Thermo Fisher Scientific) were implanted either subcutaneously in the left flank or into the left mammary fat pad of 6-week-old female NXG (NOD-Prkdc^{scid}-IL2rg^{Tm1}/Rj) mice. On day 3, when a tumor volume of 30–60 mm^3 was reached, 1×10^{11} VG of either AAV2 or AAV-αFAP-Nb encoding nanoluciferase transgene was administered intravenously per mouse ($N = 4$ per group). Nanoluciferase activity was monitored at 24 h, 7 days, and 12 days post-AAV administration using an IVIS Lumina III bioluminescence imaging system (PerkinElmer, Shelton, CT) with a CCD camera. For this purpose, 50 μL 0.88 μmol fluorofurimazine (Promega) in PBS prepared according to the manufacturer's recommendation was injected intraperitoneally into the mice 12 min before anesthetization. Light emission was measured 15 min post injection in supine position. At final necropsy, primary tumor tissues, as well as liver, heart, lung, and spleen tissues were collected and, immediately, *ex vivo* bioluminescence imaging was performed. The bioluminescence activity was read with an IVIS Lumina III bioluminescence imaging system (PerkinElmer) with a CCD camera. Next, the tissues were snap frozen and stored at −80°C for subsequent AAV tissue biodistribution analyses.

This animal study was approved by the Ethics Committee for Animal Experimentation and is registered by the regional board Freiburg. Mice are handled according to the German animal welfare law and the GV-SOLAS guidelines. Health monitoring of the animal facility is done according to FELASA guidelines quarterly by examination of sentinel animals. The animals were housed with a 12 h daylight and darkness cycle, maintained in individually ventilated cages at a temperature of 22°C ± 2°C and humidity 45%–65%, and the behavior of the animals were monitored daily throughout this study.

Tissue processing and AAV biodistribution analyses

The collected snap-frozen tissues were processed for DNA and RNA extraction. Twenty milligrams of snap-frozen tissues were disrupted and homogenized using the AllPrep DNA/RNA Mini kit Buffer RLT Plus (QIAGEN) in a Metal Bead Lysing Matrix Tube (MP). The tissues were disrupted and homogenized in a Precellys Evolution Touch homogenizer (Bertin Instruments, Montigny-le-Bretonneux, France). The homogenized lysates were centrifuged, and the supernatants were transferred to Phase Lock Gel tubes (TIANGEN, Beijing, China). Phenol-chloroform precipitation of RNA was performed by first adding phenol-chloroform-isoamylalcohol (Sigma-Aldrich, Burlington, MA), the samples were centrifuged and equal volume of chloroform-isoamylalcohol (Sigma-Aldrich) was added, and the samples were centrifuged after A short 3 min incubation. The upper phase was carefully collected and transferred to Nunc 1.0 and 2.0 mL DeepWell Plates (Thermo Fisher Scientific). A 100 μL aliquot of the collected upper phase was processed for RNA isolation following the MagMax mirVANA Total RNA Isolation Kit (Thermo Fisher Scientific) following the manufacturer's instructions. Extraction was performed using the KingFisher Flex Magnetic Particle Processor 96DW device (Thermo Fisher Scientific). For DNA extraction, 500 μL of the collected upper phase was processed using the MagMax DNA Multi-Sample Ultra 2.0 Kit (Thermo Fisher Scientific) following the manufacturer's instructions and extraction was performed using the KingFisher Flex Magnetic Particle Processor 96DW device (Thermo Fisher Scientific). For the quantification of AAV vector genome biodistribution in the tissues, 500 ng of DNA per sample was analyzed by dPCR with the AAV2 ITR-specific probes as described in the dPCR section above. In addition, nanoluciferase expression was quantified by performing dPCR using nanoluciferase-specific primer probes (forward primer: TCGACGAGCGCCT GATC, reverse primer: GGTCACTCCGTTGATGGTTACTC, probe FAM-ACCCCGACGGCTCCCTGCTG-BHQ1) (Sigma-Aldrich).

Naive VHH yeast display

Fresh whole blood was procured for six naive alpacas (*Vicugna pacos*), three naive camels (two *Camelus dromedarius* and one *Camelus bactrianus*), and 11 naive llamas (*Lama glama*). Peripheral blood mononuclear cells were isolated from each donor followed by column purification of RNA using the Monarch Total RNA Miniprep Kit (New England Biolabs, Ipswich, MA). Complementary DNA was

then synthesized using both random hexamer and oligo d(T) primers and the SuperScript IV First-Strand Synthesis System (Thermo Fisher Scientific). Variable heavy chains were amplified using an equimolar mixture of primers described by two publications[59,60] and an additional primer, Lla_FW3: CAGGCTCAGGTACAGCTGGTGGA. Primers were modified to allow for cloning into the yeast display vector, pYES3/AGA2 (modified from pYES3/CT) (Thermo Fisher Scientific) via Golden Gate Cloning. The assembled vector was electroporated into *Saccharomyces cerevisiae* yeast display strain EBY100 (ATCC), which contained a GAL1-AGA1 insertion, according to the protocol by Benatuil et al.[61] Three yeast surface display antibody libraries were constructed for each of the three pooled, naive camelid species. Selections for biotinylated human FAP consisted of two rounds of magnetic-activated cell sorting (MACS) and two rounds of fluorescence-activated cell sorting (FACS). A final round of FACS was performed to remove non-specific streptavidin binders. Both rounds of MACS were performed with antigen binding at 1 μM in 1 mL for 30 min at 4°C. For FACS, antibody expression was detected via anti-DYKDDDDK (anti-FLAG)/Alexa Fluor 488 (AF488) (R&D Systems, Minneapolis, MN) and antigen binding was detected via streptavidin/phycoerythrin (PE) (Thermo Fisher Scientific). The third round of selection was performed on 1 μM biotinylated antigen followed by a fourth round of selection on 100 nM biotinylated antigen. Libraries were immediately plated to check for unique clones. Individual colony-forming units were picked and cultured overnight before performing amplification of the heavy chain antibody for subsequent Sanger sequencing.

Statistical analysis

Statistical analyses were performed using GraphPad Prism software version 10.0 (GraphPad Software, San Diego, CA). Data are presented as mean ± standard error of the mean. Tests for statistical significance used the multiple unpaired two-tailed Student's t test. $p < 0.05$ were considered significant and $p > 0.05$ were considered non-significant and not shown.

DATA AND CODE AVAILABILITY

Supporting data for this study are available upon reasonable request from the corresponding author at francois.du_plessis@boehringer-ingelheim.com.

ACKNOWLEDGMENTS

We are grateful to Benjamin Strobel, Gudrun Zimmermann, Jenny Danner-Liskus, Christine Mayer, and Kai Zuckschwerdt for their assistance with the scale-up of AAV production and quality control for *in vivo* experiments. Our profound gratitude goes to John Park for the insightful discussions and feedback on the project, as well as for providing the FAP-expressing HT1080 cell lines. Also, we would like to thank Andy Nixon and Nikša Kastrapeli for sponsoring this collaborative research. We thank Sevim Sebnem Gizem Baytar for helping with the western blot analysis of FAP expression in HT1080-huFAP, HT1080-Neo, and HEK293T cell lines. This research was funded by the Research Beyond Borders Department, Boehringer Ingelheim Pharma GmbH & Co. KG, Biberach (Riss), Germany.

AUTHOR CONTRIBUTIONS

Conceptualization, O.O., F.d.P., and T.P.; methodology, O.O. and F.d.P.; experimental validation, O.O., F.H., P.C., and C.H.K.; formal analysis, O.O.; data curation, O.O.; writing – original draft, O.O.; writing – review & editing, O.O., F.d.P., T.P., and U.M.; supervision, F.d.P., T.P., and U.M.; project administration, O.O. All authors have read and agreed to the published version of the manuscript.

DECLARATION OF INTERESTS

O.O., F.H., P.M., U.M., and F.d.P. are employees of Boehringer Ingelheim Pharma GmbH & Co. KG, Biberach, Germany. P.C., C.K., and T.P. are employees of Boehringer Ingelheim Pharmaceuticals, Inc., Ridgefield, CT, USA.

SUPPLEMENTAL INFORMATION

Supplemental information can be found online at https://doi.org/10.1016/j.omtm.2024.101378.

REFERENCES

1. Srivastava, A., Lusby, E.W., and Berns, K.I. (1983). Nucleotide sequence and organization of the adeno-associated virus 2 genome. J. Virol. *45*, 555–564. https://doi.org/10.1128/jvi.45.2.555-564.1983.

2. Atchison, R.W., Casto, B.C., and Hammon, W.M.D. (1965). Adenovirus-Associated Defective Virus Particles. Science *149*, 754–756. https://doi.org/10.1126/science.149.3685.754.

3. Samulski, R.J., Berns, K.I., Tan, M., and Muzyczka, N. (1982). Cloning of adeno-associated virus into pBR322: Rescue of intact virus from the recombinant plasmid in human cells. Proc. Natl. Acad. Sci. USA *79*, 2077–2081. https://doi.org/10.1073/pnas.79.6.2077.

4. Laughlin, C.A., Tratschin, J.-D., Coon, H., and Carter, B.J. (1983). Cloning of infectious adeno-associated virus genomes in bacterial plasmids. Gene *23*, 65–73. https://doi.org/10.1016/0378-1119(83)90217-2.

5. Wang, D., Tai, P.W.L., and Gao, G. (2019). Adeno-associated virus vector as a platform for gene therapy delivery. Nat. Rev. Drug Discov. *18*, 358–378. https://doi.org/10.1038/s41573-019-0012-9.

6. Asokan, A., and Shen, S. (2023). Redirecting AAV Vectors to Extrahepatic Tissues. Mol. Ther. *31*, 3371–3375. https://doi.org/10.1016/j.ymthe.2023.10.005.

7. Ghauri, M.S., and Ou, L. (2023). AAV Engineering for Improving Tropism to the Central Nervous System. Biology (Basel) *12*, 186. https://doi.org/10.3390/biology12020186.

8. Dhillon, S. (2024). Fidanacogene Elaparvovec: First Approval. Drugs *84*, 479–486. https://doi.org/10.1007/s40265-024-02017-4.

9. Pupo, A., Fernández, A., Low, S.H., François, A., Suárez-Amarán, L., and Samulski, R.J. (2022). AAV vectors: The Rubik's cube of human gene therapy. Mol. Ther. *30*, 1–27. https://doi.org/10.1016/j.ymthe.2022.09.015.

10. Mingozzi, F., and High, K.A. (2011). Therapeutic *in vivo* gene transfer for genetic disease using AAV: Progress and challenges. Nat. Rev. Genet. *12*, 341–355. https://doi.org/10.1038/nrg2988.

11. Toromanoff, A., Chérel, Y., Guilbaud, M., Penaud-Budloo, M., Snyder, R.O., Haskins, M.E., Deschamps, J.Y., Guigand, L., Podevin, G., Arruda, V.R., et al. (2008). Safety and efficacy of regional intravenous (RI) versus intramuscular (IM) delivery of rAAV1 and rAAV8 to nonhuman primate skeletal muscle. Mol. Ther. *16*, 1291–1299. https://doi.org/10.1038/mt.2008.87.

12. Waehler, R., Russell, S.J., and Curiel, D.T. (2007). Engineering targeted viral vectors for gene therapy. Nat. Rev. Genet. *8*, 573–587. https://doi.org/10.1038/nrg2141.

13. Münch, R.C., Janicki, H., Völker, I., Rasbach, A., Hallek, M., Büning, H., and Buchholz, C.J. (2013). Displaying high-affinity ligands on adeno-associated viral vectors enables tumor cell-specific and safe gene transfer. Mol. Ther. *21*, 109–118. https://doi.org/10.1038/mt.2012.186.

14. Büning, H., Huber, A., Zhang, L., Meumann, N., and Hacker, U. (2015). Engineering the AAV capsid to optimize vector-host-interactions. Curr. Opin. Pharmacol. *24*, 94–104. https://doi.org/10.1016/j.coph.2015.08.002.

15. Rodríguez-Márquez, E., Meumann, N., and Büning, H. (2020). Adeno-associated virus (AAV) capsid engineering in liver-directed gene therapy. Expert Opin. Biol. Ther. *21*, 1–18. https://doi.org/10.1080/14712598.2021.1865303.

16. Li, C., and Samulski, R.J. (2020). Engineering adeno-associated virus vectors for gene therapy. Nat. Rev. Genet. *21*, 255–272. https://doi.org/10.1038/s41576-019-0205-4.

17. Lee, E.J., Guenther, C.M., and Suh, J. (2018). Adeno-associated virus (AAV) vectors: Rational design strategies for capsid engineering. Curr. Opin. Biomed. Eng. *7*, 58–63. https://doi.org/10.1016/j.cobme.2018.09.004.

18. Hamann, M.V., Beschorner, N., Vu, X.K., Hauber, I., Lange, U.C., Traenkle, B., Kaiser, P.D., Foth, D., Schneider, C., Büning, H., et al. (2021). Improved targeting of human CD4+ T cells by nanobody-modified AAV2 gene therapy vectors. PLoS One *16*, e0261269. https://doi.org/10.1371/journal.pone.0261269.

19. Eichhoff, A.M., Börner, K., Albrecht, B., Schäfer, W., Baum, N., Haag, F., Körbelin, J., Trepel, M., Braren, I., Grimm, D., et al. (2019). Nanobody-Enhanced Targeting of AAV Gene Therapy Vectors. Mol. Ther. Methods Clin. Dev. *15*, 211–220. https://doi.org/10.1016/j.omtm.2019.09.003.

20. Zdechlik, A.C., He, Y., Aird, E.J., Gordon, W.R., and Schmidt, D. (2020). Programmable Assembly of Adeno-Associated Virus-Antibody Composites for Receptor-Mediated Gene Delivery. Bioconjug. Chem. *31*, 1093–1106. https://doi.org/10.1021/acs.bioconjchem.9b00790.

21. Pham, Q., Glicksman, J., Shahraeini, S., Han, B., Jewel, D., Loynd, C., Roy, S.J.S., and Chatterjee, A. (2024). A facile chemical strategy to synthesize precise AAV-protein conjugates for targeted gene delivery. Preprint at bioRxiv. https://doi.org/10.1101/2024.07.20.604406.

22. Bao, G., Tang, M., Zhao, J., and Zhu, X. (2021). Nanobody: a promising toolkit for molecular imaging and disease therapy. EJNMMI Res. *11*, 6. https://doi.org/10.1186/s13550-021-00750-5.

23. Yang, A.T., Kim, Y.O., Yan, X.Z., Abe, H., Aslam, M., Park, K.S., Zhao, X.Y., Jia, J.D., Klein, T., You, H., and Schuppan, D. (2023). Fibroblast Activation Protein Activates Macrophages and Promotes Parenchymal Liver Inflammation and Fibrosis. Cell Mol. Gastroenterol. Hepatol. *15*, 841–867. https://doi.org/10.1016/j.jcmgh.2022.12.005.

24. Basalova, N., Alexandrushkina, N., Grigorieva, O., Kulebyakina, M., and Efimenko, A. (2023). Fibroblast Activation Protein Alpha (FAPα) in Fibrosis: Beyond a Perspective Marker for Activated Stromal Cells? Biomolecules *13*, 1718. https://doi.org/10.3390/biom13121718.

25. Scanlan, M.J., Raj, B.K., Calvo, B., Garin-Chesa, P., Sanz-Moncasi, M.P., Healey, J.H., Old, L.J., and Rettig, W.J. (1994). Molecular cloning of fibroblast activation protein α, a member of the serine protease family selectively expressed in stromal fibroblasts of epithelial cancers. Proc. Natl. Acad. Sci. USA *91*, 5657–5661. https://doi.org/10.1073/pnas.91.12.5657.

26. Burckhart, T., Thiel, M., Nishikawa, H., Wüest, T., Müller, D., Zippelius, A., Ritter, G., Old, L., Shiku, H., and Renner, C. (2010). Tumor-specific Crosslinking of GITR as Costimulation for Immunotherapy. J. Immunother. *33*, 925–934. https://doi.org/10.1097/CJI.0b013e3181f3cc87.

27. Shahvali, S., Rahiman, N., Jaafari, M.R., and Arabi, L. (2023). Targeting fibroblast activation protein (FAP): advances in CAR-T cell, antibody, and vaccine in cancer immunotherapy. Drug Deliv. Transl. Res. *13*, 2041–2056. https://doi.org/10.1007/s13346-023-01308-9.

28. Watabe, T., Liu, Y., Kaneda-Nakashima, K., Shirakami, Y., Lindner, T., Ooe, K., Toyoshima, A., Nagata, K., Shimosegawa, E., Haberkorn, U., et al. (2020). Theranostics targeting fibroblast activation protein in the tumor stroma: 64Cu- And 225Ac-labeled FAPI-04 in pancreatic cancer xenograft mouse models. J. Nucl. Med. *61*, 563–569. https://doi.org/10.2967/jnumed.119.233122.

29. Zboralski, D., Hoehne, A., Bredenbeck, A., Schumann, A., Nguyen, M., Schneider, E., Ungewiss, J., Paschke, M., Haase, C., von Hacht, J.L., et al. (2022). Preclinical evaluation of FAP-2286 for fibroblast activation protein targeted radionuclide imaging and therapy. Eur. J. Nucl. Med. Mol. Imaging *49*, 3651–3667. https://doi.org/10.1007/s00259-022-05842-5.

30. Kuklik, J., Michelfelder, S., Schiele, F., Kreuz, S., Lamla, T., Müller, P., and Park, J.E. (2021). Development of a bispecific antibody-based platform for retargeting of capsid modified aav vectors. Int. J. Mol. Sci. *22*, 8355. https://doi.org/10.3390/ijms22158355.

31. Michels, A., Frank, A.M., Günther, D.M., Mataei, M., Börner, K., Grimm, D., Hartmann, J., and Buchholz, C.J. (2021). Lentiviral and adeno-associated vectors efficiently transduce mouse T lymphocytes when targeted to murine CD8. Mol. Ther. Methods Clin. Dev. *23*, 334–347. https://doi.org/10.1016/j.omtm.2021.09.014.

32. Kern, A., Schmidt, K., Leder, C., Müller, O.J., Wobus, C.E., Bettinger, K., Von der Lieth, C.W., King, J.A., and Kleinschmidt, J.A. (2003). Identification of a Heparin-Binding Motif on Adeno-Associated Virus Type 2 Capsids. J. Virol. *77*, 11072–11081. https://doi.org/10.1128/jvi.77.20.11072-11081.2003.

33. Boucas, J., Lux, K., Huber, A., Schievenbusch, S., Von Freyend, M.J., Perabo, L., Quadt-Humme, S., Odenthal, M., Hallek, M., and Büning, H. (2009). Engineering adeno-associated virus serotype 2-based targeting vectors using a new insertion site-position 453-and single point mutations. J. Gene Med. *11*, 1103–1113. https://doi.org/10.1002/jgm.1392.

34. Muik, A., Reul, J., Friedel, T., Muth, A., Hartmann, K.P., Schneider, I.C., Münch, R.C., and Buchholz, C.J. (2017). Covalent coupling of high-affinity ligands to the surface of viral vector particles by protein trans-splicing mediates cell type-specific gene transfer. Biomaterials *144*, 84–94. https://doi.org/10.1016/j.biomaterials.2017.07.032.

35. Teschendorf, C., Warrington, K.H., Siemann, D.W., and Muzyczka, N. (2002). Comparison of the EF-1α and the CMV promoter for engineering stable tumor cell lines using recombinant adeno-associated virus. Anticancer Res. *22*, 3325–3330.

36. Mehta, A.K., Majumdar, S.S., Alam, P., Gulati, N., and Brahmachari, V. (2009). Epigenetic regulation of cytomegalovirus major immediate-early promoter activity in transgenic mice. Gene *428*, 20–24. https://doi.org/10.1016/j.gene.2008.09.033.

37. Meilinger, D., Fellinger, K., Bultmann, S., Rothbauer, U., Bonapace, I.M., Klinkert, W.E.F., Spada, F., and Leonhardt, H. (2009). Np95 interacts with *de novo* DNA methyltransferases, Dnmt3a and Dnmt3b, and mediates epigenetic silencing of the viral CMV promoter in embryonic stem cells. EMBO Rep. *10*, 1259–1264. https://doi.org/10.1038/embor.2009.201.

38. Ray, M., Tang, R., Jiang, Z., and Rotello, V.M. (2015). Quantitative Tracking of Protein Trafficking to the Nucleus Using Cytosolic Protein Delivery by Nanoparticle-Stabilized Nanocapsules. Bioconjug. Chem. *26*, 1004–1007. https://doi.org/10.1021/acs.bioconjchem.5b00141.

39. Zhang, Y., and Zhang, Z. (2020). The history and advances in cancer immunotherapy: understanding the characteristics of tumor-infiltrating immune cells and their therapeutic implications. Cell. Mol. Immunol. *17*, 807–821. https://doi.org/10.1038/s41423-020-0488-6.

40. Gogia, P., Ashraf, H., Bhasin, S., and Xu, Y. (2023). Antibody–Drug Conjugates: A Review of Approved Drugs and Their Clinical Level of Evidence. Cancers *15*, 3886. https://doi.org/10.3390/cancers15153886.

41. Riccardi, F., Dal Bo, M., Macor, P., and Toffoli, G. (2023). A comprehensive overview on antibody-drug conjugates: from the conceptualization to cancer therapy. Front. Pharmacol. *14*, 1274088. https://doi.org/10.3389/fphar.2023.1274088.

42. Wang, Y.G., Huang, P.P., Zhang, R., Ma, B.Y., Zhou, X.M., and Sun, Y.F. (2016). Targeting adeno-associated virus and adenoviral gene therapy for hepatocellular carcinoma. World J. Gastroenterol. *22*, 326–337. https://doi.org/10.3748/wjg.v22.i1.326.

43. Santiago-Ortiz, J.L., and Schaffer, D.V. (2016). Adeno-associated virus (AAV) vectors in cancer gene therapy. J. Control. Release *240*, 287–301. https://doi.org/10.1016/j.jconrel.2016.01.001.

44. Busek, P., Mateu, R., Zubal, M., Kotackova, L., and Sedo, A. (2018). Targeting Fibroblast activation protein in cancer - Prospects and caveats. Front. Biosci. *23*, 1933–1968. https://doi.org/10.2741/4682.

45. Puré, E., and Blomberg, R. (2018). Pro-tumorigenic roles of fibroblast activation protein in cancer: back to the basics. Oncogene *37*, 4343–4357. https://doi.org/10.1038/s41388-018-0275-3.

46. Garin-Chesa, P., Old, L.J., and Rettig, W.J. (1990). Cell surface glycoprotein of reactive stromal fibroblasts as a potential antibody target in human epithelial cancers. Proc. Natl. Acad. Sci. USA *87*, 7235–7239. https://doi.org/10.1073/pnas.87.18.7235.

47. Hamson, E.J., Keane, F.M., Tholen, S., Schilling, O., and Gorrell, M.D. (2014). Understanding fibroblast activation protein (FAP): Substrates, activities, expression and targeting for cancer therapy. Proteomics Clin. Appl. *8*, 454–463. https://doi.org/10.1002/prca.201300095.

48. Li, M., Younis, M.H., Zhang, Y., Cai, W., and Lan, X. (2022). Clinical summary of fibroblast activation protein inhibitor-based radiopharmaceuticals: cancer and beyond. Eur. J. Nucl. Med. Mol. Imaging *49*, 2844–2868. https://doi.org/10.1007/s00259-022-05706-y.

49. Loeffler, M., Krüger, J.A., Niethammer, A.G., and Reisfeld, R.A. (2009). Targeting tumor-associated fibroblasts improves cancer chemotherapy by increasing intratumoral drug uptake. J. Clin. Inves. *119*, 421. https://doi.org/10.1172/JCI26532C1.

50. Lee, J., Fassnacht, M., Nair, S., Boczkowski, D., and Gilboa, E. (2005). Tumor immunotherapy targeting fibroblast activation protein, a product expressed in tumor-associated fibroblasts. Cancer Res. *65*, 11156–11163. https://doi.org/10.1158/0008-5472.CAN-05-2805.

51. Hartmann, K.P., van Gogh, M., Freitag, P.C., Kast, F., Nagy-Davidescu, G., Borsig, L., and Plückthun, A. (2023). FAP-retargeted Ad5 enables *in vivo* gene delivery to stromal cells in the tumor microenvironment. Mol. Ther. *31*, 2914–2928. https://doi.org/10.1016/j.ymthe.2023.08.018.

52. Chandler, R.J., and Venditti, C.P. (2016). Gene therapy for metabolic diseases. Transl. Sci. Rare Dis. *1*, 73–89. https://doi.org/10.3233/trd-160007.

53. Crenshaw, B.J., Jones, L.B., Bell, C.R., Kumar, S., and Matthews, Q.L. (2019). Perspective on Adenoviruses: Epidemiology, Pathogenicity, and Gene Therapy. Biomedicines *7*, 61. https://doi.org/10.3390/biomedicines7030061.

54. Bulcha, J.T., Wang, Y., Ma, H., Tai, P.W.L., and Gao, G. (2021). Viral vector platforms within the gene therapy landscape. Signal Transduct. Target. Ther. *6*, 53. https://doi.org/10.1038/s41392-021-00487-6.

55. Yang, Q., Mamounas, M., Yu, G., Kennedy, S., Leaker, B., Merson, J., Wong-Staal, F., Yu, M., and Barber, J.R. (1998). Development of novel cell surface CD34-targeted recombinant adenoassociated virus vectors for gene therapy. Hum. Gene Ther. *9*, 1929–1937. https://doi.org/10.1089/hum.1998.9.13-1929.

56. Hoffmann, M.D., Gallant, J.P., LeBeau, A.M., and Schmidt, D. (2024). Unlocking precision gene therapy: harnessing AAV tropism with nanobody swapping at capsid hotspots. NAR Mol. Med. *1*, ugae008. https://doi.org/10.1093/narmme/ugae008.

57. Park, J.E., Lenter, M.C., Zimmermann, R.N., Garin-Chesa, P., Old, L.J., and Rettig, W.J. (1999). Fibroblast activation protein, a dual specificity serine protease expressed in reactive human tumor stromal fibroblasts. J. Biol. Chem. *274*, 36505–36512. https://doi.org/10.1074/jbc.274.51.36505.

58. Strobel, B., Zuckschwerdt, K., Zimmermann, G., Mayer, C., Eytner, R., Rechtsteiner, P., Kreuz, S., and Lamla, T. (2019). Standardized, Scalable, and Timely Flexible Adeno-Associated Virus Vector Production Using Frozen High-Density HEK-293 Cell Stocks and CELLdiscs. Hum. Gene Ther. Methods *30*, 23–33. https://doi.org/10.1089/hgtb.2018.228.

59. Dong, J., Thompson, A.A., Fan, Y., Lou, J., Conrad, F., Ho, M., Pires-Alves, M., Wilson, B.A., Stevens, R.C., and Marks, J.D. (2010). A single-domain llama antibody potently inhibits the enzymatic activity of botulinum neurotoxin by binding to the non-catalytic α-exosite binding region. J. Mol. Biol. *397*, 1106–1118. https://doi.org/10.1016/j.jmb.2010.01.070.

60. Ghaffari, S., Upchurch-Ange, K., Gimlin, S., Tripathi, T., Sluijter, M., Middelburg, J., van Hall, T., and Weidanz, J. (2022). A Single-Domain TCR-like Antibody Selective for the Qa-1b/Qdm Peptide Complex Enhances Tumoricidal Activity of NK Cells via Blocking the NKG2A Immune Checkpoint. J. Immunol. *208*, 2246–2255. https://doi.org/10.4049/jimmunol.2100790.

61. Benatuil, L., Perez, J.M., Belk, J., and Hsieh, C.M. (2010). An improved yeast transformation method for the generation of very large human antibody libraries. Protein Eng. Des. Sel. *23*, 155–159. https://doi.org/10.1093/protein/gzq002.